HHS Public Access

Author manuscript

Nature. Author manuscript; available in PMC 2013 April 18.

Published in final edited form as:

Nature. 2012 October 18; 490(7420): 421–425. doi:10.1038/nature11428.

A FOXO3/IRF7 gene regulatory circuit limits inflammatory sequelae of antiviral responses

Vladimir Litvak[1], **Alexander V. Ratushny**[1,2], **Aaron E. Lampano**[1], **Frank Schmitz**[1], **Albert C. Huang**[2], **Ayush Raman**[2], **Alistair G. Rust**[3], **Andreas Bergthaler**[4], **John D. Aitchison**[1,2], and **Alan Aderem**[1,5]

[1]Seattle Biomedical Research Institute, Seattle, WA 98109, USA

[2]Institute for Systems Biology, Seattle, WA 98109, USA

[3]Experimental Cancer Genetics, Welcome Trust Sanger Institute, Hinxton, Cambridge, CB10 1HH, UK

[4]Research Center for Molecular Medicine, Austrian Academy of Sciences, Lazarettgasse 14 AKH BT 25.3, 1090 Vienna, Austria

Abstract

Antiviral responses must be tightly regulated to rapidly defend against infection while minimizing inflammatory damage. Type 1 interferons (IFN-I) are crucial mediators of antiviral responses[1] and their transcription is regulated by a variety of transcription factors[2]; principal amongst these is the family of interferon regulatory factors (IRFs)[3]. The IRF gene regulatory networks are complex and contain multiple feedback loops. The tools of systems biology are well suited to elucidate the complex interactions that give rise to precise coordination of the interferon response. Here we have used an unbiased systems approach to predict that a member of the forkhead family of transcription factors, FOXO3, is a negative regulator of a subset of antiviral genes. This prediction was validated using macrophages isolated from *Foxo3*-null mice. Genome-wide location analysis combined with gene deletion studies identified the *Irf7* gene as a critical target of FOXO3. FOXO3 was identified as a negative regulator of *Irf7* transcription and we have further demonstrated that FOXO3, IRF7 and IFN-I form a coherent feed-forward regulatory circuit. Our data suggest that the FOXO3-IRF7 regulatory circuit represents a novel mechanism for establishing the requisite set points in the interferon pathway that balances the beneficial effects and deleterious sequelae of the antiviral response.

[5]Correspondence and requests for materials should be addressed to A.A. (alan.aderem@seattlebiomed.org).

Supplementary Information is linked to the online version of the paper at www.nature.com/nature.

Author contributions V.L. designed experiments, did all experimental studies and drafted the manuscript; A.V.R. did data mining and microarray data analysis; A.E.L. provided technical assistance for experiments, including quantitative real-time PCR, ChIP and *in vivo* studies; F.S. did Western blots; A.C.H. and A.R. did ChIP-Seq data analysis; A.G.R. did genome-wide motif scanning analysis; A.B. did *in vivo* studies; J.D.A. supervised the computational analysis and A.A. supervised the study and wrote the manuscript.

Author information Reprints and permissions information is available at www.nature.com/reprints. The authors declare that they have no competing financial interests.

Systems biology approaches were used to identify the gene regulatory circuits that control the anti-viral response. We combined gene expression analysis with transcription factor binding site motif scanning algorithms to infer a network of associations between transcription factors and target genes that were activated in macrophages by polyinosinic-polycytidylic acid (PIC), a widely used surrogate for dsRNA viruses that stimulates the interferon response[4] (Supplementary Fig. 1 and Supplementary Table 1). Transcription factor binding site (TFBS) motifs for IRF, STAT and FOXO transcription factors were significantly over represented within cluster 2, which includes antiviral genes like *Gbp2*, *Ccl5*, *Ifit1*, *Irf7* and *Oasl1* (Supplementary Fig. 2 and Supplementary Tables 1 and 2). Although all FOXO transcription factors bind a common DNA element[5], we decided to focus on FOXO3 since it was the sole member of the family that was significantly repressed after PIC stimulation of macrophages (Supplementary Table 3). Interestingly, the repression of *Foxo3* transcription was mirrored by increased transcription of *Irf5*, *Irf7*, *Irf8*, *Stat1*, *Stat2*, *Stat3*, and *Stat5a* genes (Supplementary Fig. 3). This result suggested that Foxo3 might act as a repressor of the IRF and STAT TFs, master regulators of the IFN-I pathways.

In order to investigate the role of FOXO3 in the regulation of the IFN-I pathway we examined the global gene expression profile in macrophages derived from *Foxo3*-null mice (Fig. 1). We detected significantly increased transcription of a subset of interferon-stimulated genes (ISG's) under basal conditions in *Foxo3*-null macrophages when compared to their wild type (WT) counterparts, suggesting that FOXO3 functions as a repressor of these genes (Fig. 1a, b and Supplementary Table 4). Stimulation of *Foxo3*-null macrophages with PIC further increased the levels of this subset of ISGs (Fig. 1c, d and Supplementary Table 5), and also revealed the transcription of additional ISGs (Fig. 1c, d and Supplementary Tables 4 and 5). The induction of these ISGs was validated by quantitative RT-PCR (Fig. 1e). Importantly, *IFNB1* itself was super-induced in PIC-stimulated macrophages from *Foxo3*-null mice (Fig. 1c, e and Supplementary Fig. 4b), suggesting the possibility that the additional subset of ISGs were regulated by autocrine feedback. In order to distinguish whether the enhanced expression of ISGs in *Foxo3*-null macrophages was due to direct effects of the transcription factor, or due to autocrine effects of the cytokine we performed genome-wide chromatin immunoprecipitation/DNA sequencing (ChIP-Seq) analysis in unstimulated macrophages as well as in macrophages stimulated by PIC. Direct FOXO3 target genes included *Cmpk2*, *Ddx58*, *Ifih1*, *Irf7*, *Mx2* and *Rsad2*, all of which have antiviral functions[1, 6] (Fig. 2b, Supplementary Fig.5 and Supplementary Table 6).

The *Irf7* gene was of particular interest because of its critical role in the establishment of the antiviral response[7], and we therefore examined the relationship between it and FOXO3 in more detail. Quantitative RT-PCR demonstrated that basal levels of *Irf7* mRNA from *Foxo3*-null macrophages were 5.5-fold higher than those in WT cells, whereas PIC-induced *Irf7* mRNA levels were similar in WT- and *Foxo3*-null cells (Fig. 1e). These results were validated by Western blot analysis (Supplementary Fig. 4a). Furthermore, deletion of FOXO3 TFBS in the *Irf7* gene promoter resulted in an increased basal *Irf7* promoter activity, and thus recapitulated the phenotype of *Foxo3*-null macrophages (Supplementary Fig. 6). These results suggest that FOXO3 functions as a negative regulator of basal *Irf7* transcription.

In order to identify the mechanism by which FOXO3 suppresses the transcription of *Irf7*, we quantified histone acetylation, ubiquitination and methylation at *Irf7* gene promoter in WT and *Foxo3*-null macrophages (Fig. 2c). Histone acetylation was significantly increased in *Foxo3*-null macrophages suggesting an epigenetic mechanism for FOXO3-mediated repression of the *Irf7* gene (Fig. 2c, d). It is worth noting that enhanced histone acetylation correlates with increased transcription of *Irf7* gene in activated macrophages (Supplementary Fig. 7). Histone acetylation is associated with an open chromatin structure that allows access of transcription factors to the DNA[8]; decreased acetylation results in the chromatin closing thereby impeding the binding of TFs to the promoter. A protein-protein interaction map[9] predicted 8 histone deacetylases that might mediate this effect (data not shown), and direct biochemical approaches including co-immunoprecipitation and ChIP-ReChIP demonstrated the existence of a ternary complex consisting of FOXO3, nuclear co-repressor 2 (NCOR2) and histone deacetylase 3 (HDAC3) on the *Irf7* promoter (Fig. 2e and Supplementary Fig. 8). A functional role for this complex is supported by the observation that treatment of macrophages with HDAC inhibitors, valproic acid (VPA) and apicidin[10], results in increased levels of *Irf7* mRNA (Supplementary Fig. 9). Most importantly, the binding of NCOR2 and HDAC3 to the *Irf7* promoter was significantly reduced in *Foxo3*-null macrophages (Fig. 2f).

In order to ascertain the transcriptional circuitry underlying the regulation of the *Irf7* gene we needed to identify all of the participating TFs. Motif scanning of the *Irf7* gene promoter predicted STAT, IRF and FOXO binding sites (Supplementary Table 7). The potential presence of the IRF site raised the possibility of auto-regulation of the *Irf7* gene by IRF7 itself, a contention supported by previous overexpression studies[11]. ChIP analysis validated the prediction that IRF7 binds to its own promoter (Fig. 2f), and importantly, FOXO3 restrained this interaction (Fig. 2g). Taken together, these results suggest a model in which a ternary complex of FOXO3, NCOR2 and HDAC3 facilitates a closed chromatin structure and limits IRF7 auto-regulation in macrophages under basal conditions (Fig. 2h).

If the FOXO3, NCOR2 and HDAC3 ternary complex keeps basal transcription of *Irf7* in check, how then does PIC-stimulation overcome this inhibition? We have observed that PIC-stimulation of macrophages results in the clearance of FOXO3, NCOR2 and HDAC3 from the *Irf7* promoter, and that this clearance is temporally associated with PIC-induced *Ifnb1* production (Fig. 2b, Supplementary Figs 8b and 10). The most plausible hypothesis is that PIC-stimulated IFN production regulates the association of FOXO3with the *Irf7* promoter. This hypothesis was confirmed by the observation that stimulation of macrophages with IFNβ induced the phosphorylation of FOXO3, and this was accompanied by a decrease in *Foxo3* mRNA and protein levels (Fig. 3a, b and Supplementary Fig. 10a). Furthermore, PIC-dependent repression of *Foxo3* mRNA and protein levels did not occur in macrophages isolated from IFN-I receptor (IFNAR1) null mice (Fig. 3a and Supplementary Fig. 10b). The decrease in mRNA levels is explained by the observation that FOXO3 is required for its own transcription (Supplementary Fig. 11). The decrease in protein levels can be explained as follows. It has previously been shown that the serine–threonine kinase AKT phosphorylates FOXO3, leading to its translocation from the nucleus and its degradation in the cytosol[12,13]. We show here that stimulation of macrophages with IFNβ

induced the phosphorylation of AKT that was accompanied by phosphorylation of FOXO3 at the Thr32 residue, a known AKT phosphorylation site (Fig. 3b). Furthermore, treatment of the cells with AKT inhibitor IV abrogated IFN-I-dependent AKT and FOXO3 phosphorylation and prevented IFN-I-mediated decrease in *Foxo3* mRNA and protein levels (Fig. 3b, c and Supplementary Fig. 10c). Taken together, these results suggest that IFN-I activates the PI3K/AKT pathway, which in turn leads to FOXO3 degradation and to the cessation of *Foxo3* transcription.

FOXO3 has been shown to control CTLA-4 mediated regulation of IL-6, TNFα, MCP-1 and IFNγ in dendritic cells[14,15,16], and this was proposed to occur via increased transcription of superoxide dismutase (SOD2)[15]. This mechanism does not appear to function in FOXO3-mediated repression of antiviral responses in macrophages since no differences in *Sod2* mRNA levels in *Foxo3*-null macrophages were detected (data not shown). Taken together, the data suggest that FOXO3 acts in a coherent feed-forward loop, thereby modulating the antiviral response (Fig. 3d). Under basal conditions FOXO3 activity serves to limit *Irf7* expression (I). IFN-I induces the transcription of *Irf7*[17]; this represents the direct, rapid, arm of the feed-forward motif (II). Concomitantly, IFN-I inhibits the transcription of *Foxo3* (III), which leads to the depletion of FOXO3 and alleviates the repression of *Irf7*. This represents the indirect, slow, arm of the feed-forward motif. Thus activation of both arms of the feed-forward motif is required to achieve the high level of IRF7 that is essential for the maximal antiviral response. In addition, this feed-forward pathway is aided by positive feedback regulation of IRF7 on IFN-I (IV) (Supplementary Fig. 12), and by positive auto-regulation of IRF7 (V). By limiting the transcription of *Irf7*, FOXO3 prevents leakiness of IRF7-induced genes in the absence of a viral infection. In addition, FOXO3 prevents spurious noise in the activity of IFN-I since it is capable of dampening the IRF7-induced positive feedback on IFN-I production.

A fine balance exists between optimal immune clearance of a virus and the collateral damage that is inflicted on infected tissue during the host response. The FOXO3-IRF7 regulatory circuit represents an ideal mechanism for balancing host defense with inflammatory damage. Since we discovered and explored the FOXO3-IRF7 regulatory circuit in macrophages we needed an *in vivo* model system in which macrophages are the principal cells that produce IFN-I in a viral infection. The vesicular stomatitis virus (VSV)-lung infection model fully meets this criterion since it has been shown that alveolar macrophages are the primary interferon producers to intranasal infection, and that this response is cell intrinsic since depletion of alveolar macrophages completely ablates host defense to the virus[18]. Furthermore, VSV is an RNA virus[19] which triggers similar pathways to PIC and which is controlled in an IRF7-dependent manner[7]. Intranasal infection of WT mice resulted in a low-grade inflammatory response by day two following infection that was accompanied by intermediate viral load (Fig. 4a-c). By day five the inflammatory response had resolved and viral titers were at basal levels (Fig. 4a-c). By contrast, *Foxo3*-null mice had significantly decreased viral loads at day two when compared with WT mice (Fig. 4b, c); however, this response was accompanied by significant lung pathology including pronounced neutrophil influx, hemorrhage and tissue damage (Fig. 4a and Supplementary Fig. 13). The virus was cleared by day five and lung inflammation was mostly resolved (Fig.

4a-c). Finally, viral replication was not controlled in *Irf7*-null mice (Fig. 4b, c). By day five these mice had developed severe pulmonary edema and were sacrificed (Fig. 4a).

As discussed above, we chose the VSV model system since the anti-viral response is intrinsic to alveolar macrophages[18]. Consistent with this, we demonstrated that alveolar macrophages, isolated from VSV infected *Foxo3*-null animals, expressed considerably greater levels of mRNA encoding *Irf7*, *Ifnb1*, and other inflammatory cytokines including *Ccl5*, *Ccl7* and *Ccl12* than their WT counterparts (Supplementary Fig. 14 and data not shown). The increased basal levels of *Irf7* mRNA in *Foxo3*-null alveolar macrophages further support a cell intrinsic role for FOXO3, although it is formally possible that other targets are also involved. A recent study demonstrated a cell intrinsic increase in CD8 T cell expansion in *Foxo3*-null mice[20]. We detected comparable T cell numbers in the lungs of VSV-infected WT and *Foxo3*-null mice, suggesting that T cells are not contributing to the phenotype (data not shown). The data presented above is consistent with the proposed role of the FOXO3/IRF7 circuit in host defense against viruses. The model predicts that FOXO3 suppresses the IRF7-dependent antiviral response in order to curb the collateral damage associated with host defense. We argue that the dynamic interplay between FOXO3, IRF7 and IFN-I, optimizes the antiviral response to achieve the appropriate balance between host defense and rampant inflammation.

Methods Summary

Cell culture

BMMs were isolated from C57BL/6, *Foxo3*-/- *Irf7*-/- and *Ifnar1*-/- mice essentially as described[21]. BMMs collected from femurs were plated on non–tissue culture–treated plastic in complete RPMI medium containing 10% (vol/vol) FBS (Hyclone Laboratories), 2 mM L-glutamine, 100 IU/ml of penicillin and 100 g/ml of streptomycin (all from Cellgro, Mediatech) and supplemented with recombinant human macrophage colony-stimulating factor (50 ng/ml; Peprotech). BMMs were treated for various length of time with high-purity LPS (10 ng/ml; *Salmonella minnesota*; List Biologicals), Pam_3CSK_4 (300ng/ml; EMC Microcollections), PIC (6μg/ml; Amersham), purified murine IFNβ (1.45×10^{-9} U/ml; PBL-interferon source), VPA (5mM; Sigma), Apicidin (2.5μM; Sigma), Ly294002 (50μM; Sigma) and AKT inhibitor IV (20μM; EMD Chemicals).

Microarrays and qRT-PCR

RNA isolation for transcriptome analysis of BMMs was performed using the Trizol reagent (Invitrogen). Gene expression profiling was performed using Affymetrix GeneChip Mouse Genome 430 2.0 and GeneChip Mouse Exon 1.0 ST arrays. Details of the analytical methods are provided in the Methods. For qRT-PCR, total RNA was reverse transcribed to complementary DNA and amplified using primers specific for murine transcripts. Expression values were calculated relative to the *Eef1a1* mRNA transcripts.

ChIP-Seq and ChIP

For ChIP-Seq, immunoprecipitated DNA samples were sequenced on a Illumina HiSeq 2000 sequencing system and aligned using the ELAND software package (Illumina). Peaks

identification was performed according to standard methods and is described in full in Methods. For quantitative ChIP, immunoprecipitated DNA samples were amplified with target promoter-specific primers.

Full Methods

Mice

C57BL/6 mice were obtained from Jackson Laboratories. *Ifnar1*-/-[22] and *Irf7*-/-[23] mice were obtained through the Swiss Immunological Mutant Mouse Repository (Zurich, Switzerland). *Foxo3*-/- mice in the FVB background[24] were obtained from MMRRC and were backcrossed to C57BL/6 mice at least 5 times to generate congenic mice. C57BL/6 *Foxo3*+/- heterozygotes were intercrossed to generate *Foxo3*-/- mice. Mice were maintained at the animal facility of the Institute for Systems Biology and used at 8–12 weeks of age. All animals were housed and handled according to the approved protocols of University of Washington and Institute for Systems Biology's Institutional Animal Care and Use Committees.

Microarray analysis

Total RNA was extracted using a Trizol solution (Invitrogen) and overall RNA quality was analyzed with an Agilent 2100 Bioanalyzer. Sample mRNA was amplified, labeled and hybridized to GeneChip Mouse Genome 430 2.0 and GeneChip Mouse Exon 1.0 ST arrays according to the array manufacturer's instructions (Affymetrix). Probe intensities were measured and then processed with Affymetrix GeneChip operating software into image analysis (.CEL) files. The Affymetrix CEL files were normalized with robust multiarray average expression measure[25] and baseline scaling using the software Bioconductor[26], then exported to Matlab (MathWorks, Natick, MA) for further analysis. The raw data from Affymetrix GeneChip Mouse Genome 430 2.0 arrays are posted at ArrayExpress[27] (http://www.ebi.ac.uk/arrayexpress/) with accession number E-TABM-310. Statistical analysis and data post-processing were performed with in-house developed functions in Matlab. For transcriptome analysis of TLR-induced responses in wild-type, *Foxo3*-/- and *Irf7*-/- BMMs, genes were selected for inclusion based on filtering for minimum $\log_2$ expression intensity (> 6) in at least one time point. Genes having differential expression (3-fold up- or down-regulated relative to wild-type unstimulated BMMs, in at least one time point) were selected for gene-clustering analysis to identify groups of genes that were co-expressed across the diverse set of TLR-stimulation experiments in wild-type BMMs, based on the assumption that genes within a cluster are likely to share common *cis*-regulatory elements[28]. Gene cluster analysis was performed using the K-means algorithm with squared Euclidean distance[29], with 500 iterations. Expression measurements were transformed based on a single universal reference experiment (wild-type unstimulated BMMs) so that the transformed measurements would all lie between -1 and 1, with zero indicating the intensity in the reference experiment[30].

Gene set enrichment analysis (GSEA)

GSEA is an analytical tool for relating differentially regulated genes to transcriptional signatures and molecular pathways associated with known biological functions[31]. The

statistical significance of the enrichment of known transcriptional signatures in a ranked list of genes was determined as described[31]. To assess the phenotypic association with FOXO3 deficiency, we used the list of genes that was ranked according to differential gene expression in *Foxo3*-/- and *Foxo3*+/+ BMMs. We used 1,294 gene sets from the Molecular Signature Database C2 version 2.5 and 24 custom gene sets including interferon-stimulated gene set (Supplementary Table 8).

Quantitative real-time PCR

For measurement of the expression of mRNA transcripts in BMMs, total RNA was collected by Trizol (Invitrogen). RNA was reverse-transcribed and analyzed by real-time PCR with TaqMan Gene Expression assays (Applied Biosystems). Data were acquired using a 7900HT Fast Real-Time PCR system (Applied Biosystems) and CF×96 Real-Time PCR Detection System (BioRad) and were normalized to the expression of *Eef1a1* mRNA transcripts (encoding eukaryotic translation elongation factor 1 α1) in individual samples. Taqman primers are listed in Supplementary Table 9.

Western blots

Whole cell extracts of BMMs and immunoprecipitations were prepared as previously described[32]. Proteins were analyzed by SDS-PAGE and subsequently by Western blot using the following antibodies against: FOXO3 (75D8) (Cell Signaling); phospho-FOXO3 (T32) (Cell Signaling); beta-actin (ab20272) (Abcam); IRF7 (Invitrogen); phospho-AKT (T308) (C31e5e) and AKT (C67e7) (Cell Signaling). Densitometric quantification of western blot bands was performed using the NIH Image J software.

Elisa

BMMs were treated for various lengths of time with PIC (6μg/ml) and supernatants were harvested and analyzed by ELISA to measure production of IFNβ (PBL Biomedical Laboratories, Piscataway, NJ).

Motif scanning

Promoter sequences encompassing 3kb on either side of the transcriptional start site of a gene were scanned using the software tool MotifLocator[33] as described[21]. Briefly, a total of 390 murine transcription factor matrices were obtained from the TRANSFAC database Professional version 9.3[34]. These matrices were used to scan gene promoters where the individual matrix thresholds were set to report predictions above the percentile of 0.067%, i.e. an expectation of observing a prediction for a matrix every 1500bp. For a pair-wise enrichment of transcription factors (TF_i) in promoter regions of a particular cluster of genes, we calculated a cumulative relative number of a TF pair ($S_l^{(TF_i,TF_j)}$) as follows

$$S_l^{(TF_i,TF_j)} = \frac{\sum_{k=1}^{N_l} M_K^{(TF_i,TF_j)}}{N_l}, \quad (1)$$

where l is the gene cluster index ($l \in \{1, \ldots, N\}$), N is the number of gene clusters, N_l is the number of genes in cluster l, $M_k^{(TF_i,TF_j)}$ is the number of predicted ($P \leq 10^{-3}$) TF binding site pairs for TF_i and TF_j. The enrichment score $(ES_l^{(TF_i,TF_j)})$ for a (TF_i,TF_j),Tnscription factor pair was calculated as follows

$$ES_l^{(TF_i,TF_j)} = \frac{S_l^{(TF_i,TF_j)}}{\max(S_k^{(TF_i,TF_j)})}, \quad (2)$$

where k is the gene cluster index ($k \in \{1, \ldots, N\}$ [$-i$]) $ES_l^{(TF_i,TF_j)}$ reflects a specific enrichment of the (TF_i, TF_j) transcription factor pair across gene clusters of interest.

ChIP-Seq and quantitative chromatin immunoprecipitation (ChIP)

For ChIP-Seq analysis formalin-fixed cells were sonicated and processed for immunoprecipitation essentially as described[17]. Briefly, 1.5×10^7 BMMs were crosslinked for 10 min. in 1% paraformaldehyde, washed and lysed. Chromatin was sheared by sonication (5 × 60 s at 30% maximum potency) to fragments of approximately 150bp. The sheared chromatin was incubated with anti-rabbit IgG Dynabeads (Invitrogen) pre-conjugated with antibodies to FOXO3 (H-144), HDAC3 (sc-11417) (Santa Cruz Biotechnology); IRF7 (Invitrogen), ubH2B (5546), ubH2A (8240), H3K36me3 (4909), H3K4me3 (9727) and H3K4me2 (9726) (Cell signaling); H3K9me (ab8896) and H3K9me3 (ab8898) (Abcam); NCOR2 (PA1-843) (Thermo Scientific) and acH4 (06-598) (Upstate), washed and eluted. The eluted chromatin was reverse-cross-linked, and DNA was purified using phenol/chloroform/isoamyl extraction. The purified ChIP DNA was prepared for sequencing with the Illumina ChIPSeq Sample Prep kit and processed in according to the manufacturer's protocol.

The ChIP-Seq data was aligned to the mouse genome (NCBI37/mm9; July 2007) using the ELAND alignment software (Illumina). Regions where the ChIP signals were enriched relative to the normal rabbit serum (NRS) control were determined as described[35]. We used a false discovery rate of less than 1%. For quantitative ChIP, immunoprecipitated DNA samples were amplified with target promoter–specific primers using Taqman quantitative PCR analysis. DNA region lacking FOXO binding sites served as a negative control[36]. Primers and probe sequences are listed in Supplementary Table 10.

Viral pathogenesis in mice

8–12 weeks old female mice were used in this study. Baseline body weights were measured before infection. Body weight and survival were monitored daily for 5 days and mice with body weight loss of more than 25% of pre-infection values were euthanized. For virological and pathological examinations, 6 mice per group were anaesthetized with ketamine/xylazine and intranasally infected with 10^5 p.f.u. (30μl) of VSV serotype Indiana (Mudd-Summers isolate), originally obtained from Dr. D. Kolakofsky (University of Geneva, Geneva, Switzerland). The virus titers in lungs were determined by standard plaque assays in Vero cells, as described[37] and by measurement of *VSVg* mRNA levels in lung samples using

quantitative real-time PCR assay. The primers used for the detection of *VSVg* mRNA were: Forward, 5′-CCTGGGTTTTTAGGAGCAAGATAG-3′; Reverse, 5′-AAGAAACCTGGAGCAAAATCAGA-3′ and FAM labeled probe, 5′-CGGGTCTTCCAATCTCTCCAGTGGATCT-3′

To assess viral pathogenesis, lungs of control and experimentally infected mice were processed for haematoxylin and eosin staining. In addition to determine the extent of neutrophil influx, the lung samples were processed for immunohistochemistry staining with antibodies against LY6B (Serotec).

Luciferase Assay

RAW 264.7 cells were transfected with *Irf7*- and *Foxo3*-promoter luciferase reporter constructs, and with constitutively active FOXO3 (FOXO3-TM) construct obtained from Addgene (plasmid 1788)[12]. Luciferase assays were performed as described[38]. All luciferase activity was normalized to the expression of the co-transfected Renilla luciferase.

Supplementary Material

Refer to Web version on PubMed Central for supplementary material.

Acknowledgments

We thank Kathleen A. Kennedy and Jacques J. Peschon for discussions and critical reading of the manuscript; and Samuel A. Danziger, Tetyana Stolyar and Elena van Gaver for technical assistance. This work was supported by grants and contracts from the National Institutes of Health R01AI025032, R01AI032972, HHSN272200700038C, HHSN272200800058C and U54GM103511. Microarray and ChIP-Seq raw data have been submitted to the Gene Expression Omnibus under accession number GSE37052.

References

1. Liu SY, Sanchez DJ, Cheng G. New developments in the induction and antiviral effectors of type I interferon. Curr Opin Immunol. 2011; 23:57–64. [PubMed: 21123041]
2. Panne D, Maniatis T, Harrison SC. An atomic model of the interferon-beta enhanceosome. Cell. 2007; 129:1111–1123. [PubMed: 17574024]
3. Tamura T, Yanai H, Savitsky D, Taniguchi T. The IRF family transcription factors in immunity and oncogenesis. Annu Rev Immunol. 2008; 26:535–584. [PubMed: 18303999]
4. Barbalat R, Ewald SE, Mouchess ML, Barton GM. Nucleic Acid Recognition by the Innate Immune System. Annu Rev Immunol. 2011; 29:185–214. [PubMed: 21219183]
5. Benayoun BA, Caburet S, Veitia RA. Forkhead transcription factors: key players in health and disease. Trends Genet. 2011; 27:224–232. [PubMed: 21507500]
6. Schoggins JW, et al. A diverse range of gene products are effectors of the type I interferon antiviral response. Nature. 2011; 472:481–485. [PubMed: 21478870]
7. Honda K, et al. IRF-7 is the master regulator of type-I interferon-dependent immune responses. Nature. 2005; 434:772–777. [PubMed: 15800576]
8. Shahbazian MD, Grunstein M. Functions of Site-Specific Histone Acetylation and Deacetylation. Annu Rev Biochem. 2007; 76:75–100. [PubMed: 17362198]
9. Szklarczyk D, et al. The STRING database in 2011: functional interaction networks of proteins, globally integrated and scored. Nucleic Acids Res. 2011; 39:D561–D568. [PubMed: 21045058]
10. Khan N, et al. Determination of the class and isoform selectivity of small-molecule histone deacetylase inhibitors. Biochem J. 2008; 409:581–589. [PubMed: 17868033]

11. Ning S, Huye LE, Pagano JS. Regulation of the transcriptional activity of the IRF7 promoter by a pathway independent of interferon signaling. J Biol Chem. 2005; 280:12262–12270. [PubMed: 15664995]
12. Brunet A, et al. Akt promotes cell survival by phosphorylating and inhibiting a Forkhead transcription factor. Cell. 1999; 96:857–868. [PubMed: 10102273]
13. Plas DR, Thompson CB. Akt activation promotes degradation of tuberin and FOXO3a via the proteasome. J Biol Chem. 2003; 278:12361–12366. [PubMed: 12517744]
14. Dejean AS, et al. Transcription factor Foxo3 controls the magnitude of T cell immune responses by modulating the function of dendritic cells. Nat Immunol. 2009; 10:504–513. [PubMed: 19363483]
15. Fallarino F, et al. CTLA-4-Ig activates forkhead transcription factors and protects dendritic cells from oxidative stress in nonobese diabetic mice. J Exp Med. 2004; 200:1051–1062. [PubMed: 15492127]
16. Wang ST, et al. RNA interference-mediated silencing of Foxo3 in antigen-presenting cells as a strategy for the enhancement of DNA vaccine potency. Gene Ther. 2011; 18:372–383. [PubMed: 21107437]
17. Ning S, Pagano JS, Barber GN. IRF7: activation, regulation, modification and function. Genes Immun. 10.1038/gene.2011.21
18. Kumagai Y, et al. Alveolar macrophages are the primary interferon-alpha producer in pulmonary infection with RNA viruses. Immunity. 2007; 27:240–252. [PubMed: 17723216]
19. Lyles, DS.; Rupprecht, CE. Fields Virology. 5th. Howley, PM.; Knipe, DM., editors. Vol. 1. 2007. p. 1363-1408.
20. Sullivan JA, Kim EH, Plisch EH, Peng SL, Suresh M. FOXO3 regulates CD8 T cell memory by T cell-intrinsic mechanisms. PLoS Pathog. 2012; 8(2):e1002533. [PubMed: 22359505]
21. Gilchrist M, et al. Systems biology approaches identify ATF3 as a negative regulator of Toll-like receptor 4. Nature. 2006; 441:173–178. [PubMed: 16688168]
22. Muller U, et al. Functional role of type I and type II interferons in antiviral defense. Science. 1994; 264:1918–1921. [PubMed: 8009221]
23. Honda K, et al. IRF-7 is the master regulator of type-I interferondependent immune responses. Nature. 2005; 434:772–777. [PubMed: 15800576]
24. Castrillon DH, Miao L, Kollipara R, Horner JW, DePinho RA. Suppression of ovarian follicle activation in mice by the transcription factor Foxo3a. Science. 2003; 301(5630):215–8. [PubMed: 12855809]
25. Irizarry RA, et al. Exploration, normalization, and summaries of high density oligonucleotide array probe level data. Biostatistics. 2003; 4:249–264. [PubMed: 12925520]
26. Gentleman RC, et al. Bioconductor: open software development for computational biology and bioinformatics. Genome Biol. 2004; 5 research80.
27. Parkinson H, et al. ArrayExpress--a public database of microarray experiments and gene expression profiles. Nucleic Acids Res. 2007; 35:D747–D750. [PubMed: 17132828]
28. Chiang DY, Brown PO, Eisen MB. Visualizing associations between genome sequences and gene expression data using genome-mean expression profiles. Bioinformatics. 2001; 17:S49–S55. [PubMed: 11472992]
29. Dollar, P. Piotr Dollar's Image and Video Toolbox for Matlab. San Diego, CA: University of California, San Diego; 2006.
30. Ramsey SA, et al. Uncovering a macrophage transcriptional program by integrating evidence from motif scanning and expression dynamics. PLoS Comput Biol. 2008; 21:e1000021. [PubMed: 18369420]
31. Subramanian A, et al. Gene set enrichment analysis: a knowledge-based approach for interpreting genome-wide expression profiles. Proc Natl Acad Sci U S A. 2005; 102:15545–15550. [PubMed: 16199517]
32. Gilchrist M, McCauley SD, Befus AD. Expression, localization, and regulation of NOS in human mast cell lines: effects on leukotriene production. Blood. 2004; 104:462–469. [PubMed: 15044250]

33. Thijs G, et al. INCLUSive: integrated clustering, upstream sequence retrieval and motif sampling. Bioinformatics. 2002; 18:331–332. [PubMed: 11847086]
34. Biobase. TRANSFAC Professional v9.3. Available at: http://www.biobase.de
35. Ramsey SA, et al. Genome-wide histone acetylation data improve prediction of mammalian transcription factor binding sites. Bioinformatics. 2010; 26:2071–2075. [PubMed: 20663846]
36. Renault VM, et al. FoxO3 regulates neural stem cell homeostasis. Cell Stem Cell. 2009; 6:527–539. [PubMed: 19896443]
37. McCaren L, Holland JJ, Syverton JT. The mammalian cell–virus relationship. I. Attachment of poliovirus to cultivated cells of primate and non-primate origin. J Exp Med. 1959; 109:475–485. [PubMed: 13641571]
38. Smith KD, et al. Toll-like receptor 5 recognizes a conserved site on flagellin required for protofilament formation and bacterial motility. Nat Immunol. 2003; 4:1247–1253. [PubMed: 14625549]

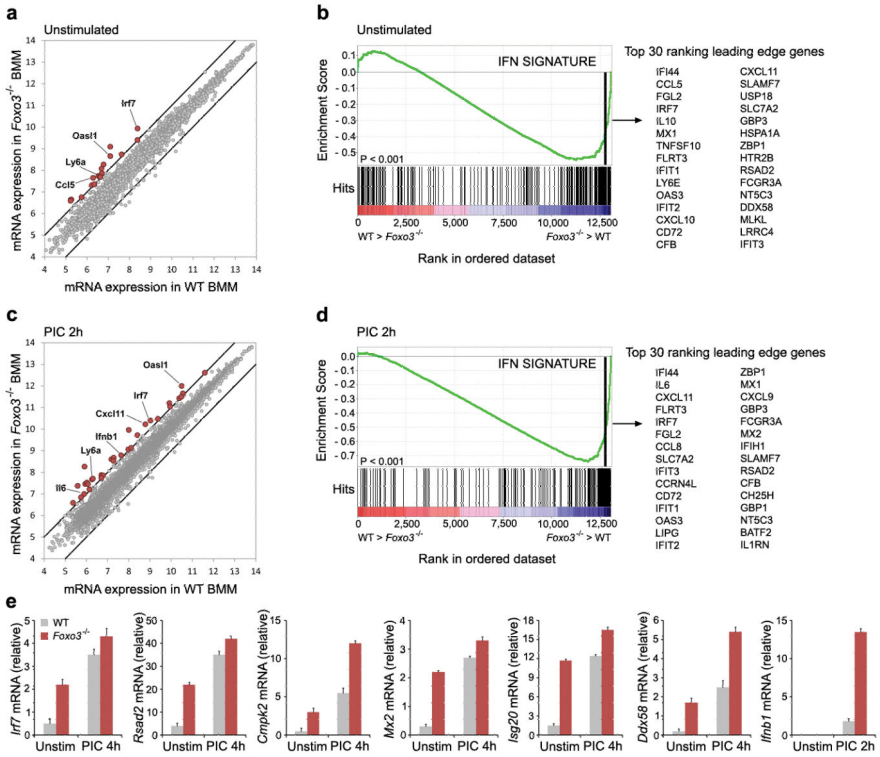

Figure 1. FOXO3 is a negative regulator of the antiviral response

a, Scatter plot comparing global gene expression profiles between unstimulated WT and *Foxo3*-null BMMs. The black lines indicate a two-fold cutoff for the difference in gene expression levels. Data represent the average of three independent experiments. mRNA expression levels are on the $\log_2$-scale. **b**, Gene-set enrichment analysis (GSEA) reveals the overrepresentation of IFN transcriptional signature genes in unstimulated *Foxo3*-null BMMs. Genes are ranked into an ordered list based on relative expression in wild type and *Foxo3*-null BMMs. The middle part of the plot shows the distribution of the genes in the IFN transcriptional signature gene set ("Hits") against the ranked list of genes. The list on the right shows the top 30 genes in the leading edge subset. Data represent the average of three independent experiments. **c**, Global gene expression in PIC-stimulated WT and *Foxo3*-null BMMs was analyzed as in **a. d**, Gene-set enrichment analysis demonstrates up-regulation of IFN transcriptional signature in PIC-stimulated *Foxo3*-null BMMs. Data represent the average of three independent experiments. **e**, mRNA levels of *Cmpk2*, *Ddx58*, *Irf7*, *Isg20*, *Mx2*, *Rsad2* and *Ifnb1* in WT and *Foxo3*-null macrophages in the presence or absence of PIC stimulation. Data are representative of three experiments (average of three values ± standard error).

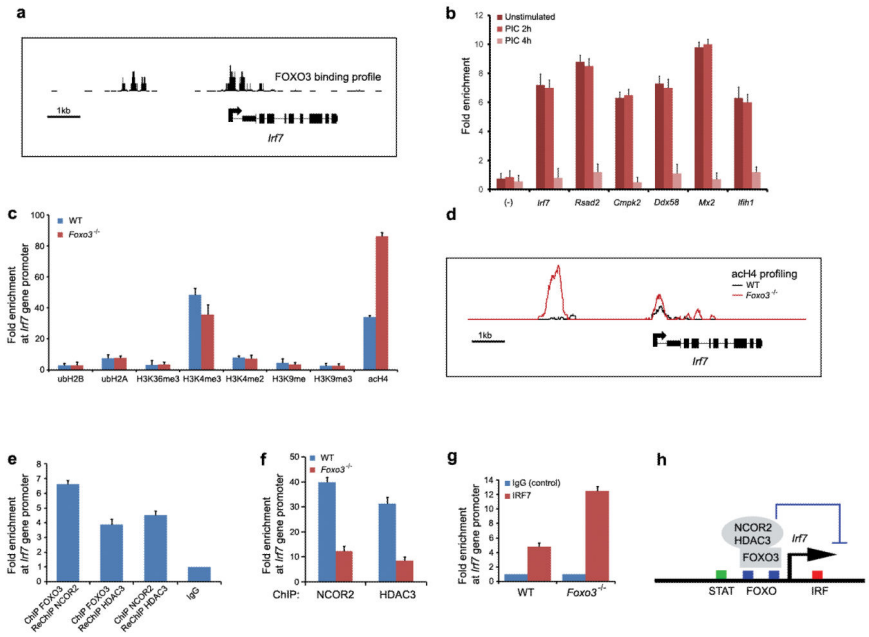

Figure 2. FOXO3 keeps the *Irf7*gene in check

a, ChIP-Seq analysis demonstrates FOXO3 binding profile at *Irf7* gene promoter in wild type BMMs. Data are representative of two experiments. **b**, ChIP of FOXO3 from unstimulated wild-type macrophages shows binding of FOXO3 to the promoters of the target genes. FOXO3 recruitment was not observed at control regions lacking FOXO binding sites (-). Data was normalized to IgG (negative control) and represent the average of three independent experiments ± standard error. **c**, ChIP analysis of histone acetylation, ubiquitination and methylation at *Irf7* gene promoter in WT and *Foxo3*-null macrophages. Data represent the average of three independent experiments (± standard error). **d**, ChIP-Seq analysis demonstrates increased histone H4 acetylation levels in *Foxo3*-null cells. Data are representative of two experiments. **e**, FOXO3, NCOR2 and HDAC3 are present in the ternary complex at *Irf7* promoter, as shown by ChIP-ReChIP assays in unstimulated BMMs. Data was compared to IgG and represent the average of three independent experiments ± standard error. **f**, ChIP analysis of NCOR2 and HDAC3 binding at *Irf7* gene promoter in WT and *Foxo3*-null macrophages. Data represent the average of three independent experiments (± standard error). **g**, ChIP assay demonstrates increased recruitment of IRF7 at *Irf7* gene promoter in *Foxo3*-null macrophages relative. Data was normalized to IgG and represent the average of three independent experiments ± standard error. **h**, A model depicting the mechanism of FOXO3-mediated repression of *Irf7* gene. See text for details.

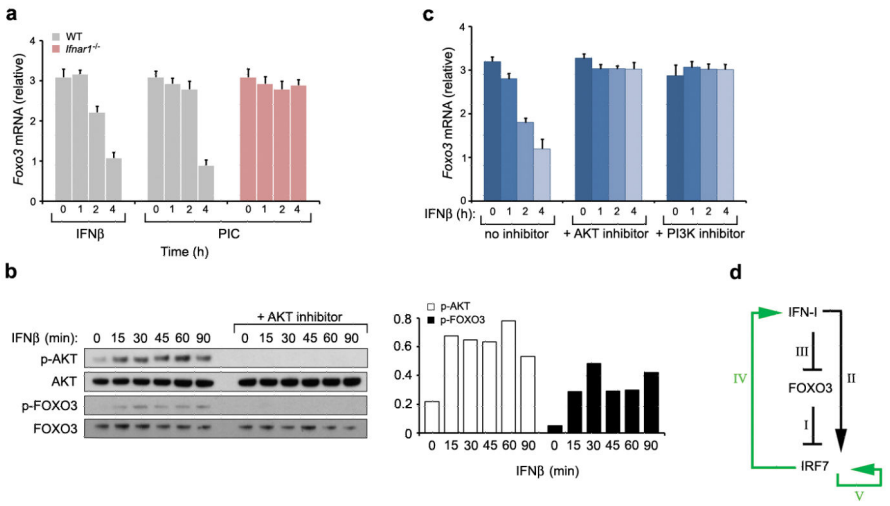

Figure 3. IFNβ represses FOXO3

a, IFNβ- or PIC-stimulation of wild type macrophages was associated with a significant decrease in *Foxo3* mRNA levels. PIC-induced decrease of *Foxo3* mRNA levels was not observed in *Ifnar1*-null cells. Data are representative of three experiments (average of three values ± standard error). **b**, IFNβ induces activation of AKT in macrophages. Bar graph demonstrates densitometric quantification of phosphorylated AKT and FOXO3 protein levels. **c**, IFNβ-induced repression of *Foxo3* mRNA levels in WT BMMs was measured in the presence and absence of PI3K and AKT inhibitors. Data are representative of three experiments (average of three values ± standard error). **d**, A model depicting FOXO3/IRF7/IFN-I regulatory circuit. See text for details.

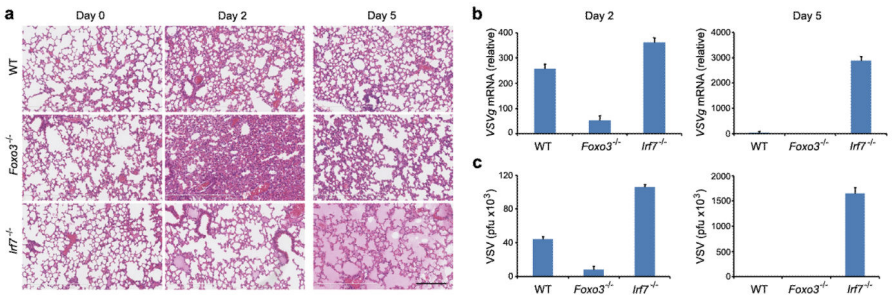

Figure 4. Antiviral responses lead to increased lung injury in the absence of FOXO3 and IRF7

a, H&E staining of lung tissue sections from wild-type, *Foxo3*-null and *Irf7*-null mice 0, 2 and 5 days after intranasal infection with VSV serotype Indiana 10^5 p.f.u. Data are from one experiment that is representative of three independent experiments (n=6 mice per group). Scale bar, 200μm. The viral burden in lungs was determined by measurement of *VSVg* mRNA levels in lung samples using quantitative real-time PCR assay **(b)** and by standard plaque assays in Vero cells **(c)**. Data are representative of three experiments (average of three values ± standard error).